

Simple adaptive re-entry guidance for path-constraint tracking

Mooij, E.

DOI 10.2514/6.2018-1318

Publication date

Document Version Accepted author manuscript Published in AIAA Guidance, Navigation, and Control

Citation (APA)

Mooij, E. (2018). Simple adaptive re-entry guidance for path-constraint tracking. In *AIAA Guidance, Navigation, and Control* (210039 ed.). Article AIAA 2018-1318 American Institute of Aeronautics and Astronautics Inc. (AIAA). https://doi.org/10.2514/6.2018-1318

Important note

To cite this publication, please use the final published version (if applicable). Please check the document version above.

Other than for strictly personal use, it is not permitted to download, forward or distribute the text or part of it, without the consent of the author(s) and/or copyright holder(s), unless the work is under an open content license such as Creative Commons.

Takedown policy

Please contact us and provide details if you believe this document breaches copyrights. We will remove access to the work immediately and investigate your claim.



AIAA-18-1318

Simple Adaptive Re-entry Guidance for Path-Constraint Tracking

E. Mooij

Delft University of Technology, Delft, The Netherlands



AIAA Guidance, Navigation, and Control ConferenceJanuary 8-12, Kissimmee, FL

Simple Adaptive Re-entry Guidance for Path-Constraint Tracking

E. Mooij*

Delft University of Technology, Faculty of Aerospace Engineering, Kluyverweg 1, 2629 HS Delft, The Netherlands

To limit the mass of the vehicle's thermal protection system, an optimal trajectory that minimises the total integrated heat load should be flown. This means that the maximum heat-flux constraint is followed for as long as possible, until the maximum mechanical load is encountered. Flying as close to this load as possible contributes to minimising the heat load as well. The guidance system to track the path constraints includes three components: a semi-analytical guidance that produces nominal bank-angle commands, an inner-loop tracking system based on linearised output feedback, and an outer-loop system based on simple adaptive control to remove the remaining error. The former two guidance components have been taken from an earlier design, and the performance gain after adding the adaptive system is studied here in detail. The flight system under consideration is a hypersonic test vehicle of which the stagnation heat-flux should not exceed 1,700 kW/m², with a limit of the mechanical load of 5g. The results show that the adaptive tracking system extends the duration of heat-flux tracking and is able to track tighter at even less guidance effort, but reduces the flight range because of that. A simultaneous optimisation of these two conflicting objectives should be pursued to refine the guidance-system design in case both have requirements to be met. In none of the cases considered, the g-load constraint was violated, although a more detailed analysis is required to make this part of the guidance more robust. In all other aspects, the combination of an inner-loop and outer-loop tracking has made the path-constraint tracking more robust and keeps the errors below acceptable levels.

Nomenclature

${f A}$	system matrix
a_{γ}	normal acceleration other than from vertical lift, m/s ²
a	speed of sound, m/s
\mathbf{B}	control matrix
\mathbf{C}	output matrix
c_1	heat-flux constant
c_2	heat-flux exponent
C_D	drag coefficient
C_L	lift coefficient
c_n	value of $\rho V^n = \text{constant}$
c_{γ}	gain constant, s/rad
d_{total}	total flight range, m
D	drag, N
e_{γ}	flight-path angle error, rad
f_{n_q}	transition percentage for g -load
g	gravitational acceleration, m/s ²
H_s	atmospheric scale height, m
h	altitude, m

^{*}Assistant Professor, section Astrodynamics and Space Missions, e.mooij@tudelft.nl, Associate Fellow AIAA.

```
h^*
           pseudo altitude, m
\mathbf{K}
           gain matrix
K
           ballistic parameter, N/m<sup>2</sup>
K_{\gamma}
           flight-path angle gain, various (subscripts p, i, and d for the PID compensator)
K_n
           bank-angle gain, various (subscripts p and d for the PD compensator)
L
           lift, N
M
           Mach number
m
           mass, kg
           exponent in nominal-guidance law (n_1 = 6 \text{ for heat flux, and } n_2 = 2 \text{ for } g\text{-load})
n
n_g
           q-load
\mathbf{Q}
           state-deviation weighing matrix
Q
           integrated heat load, J/m<sup>2</sup>
           convective heat flux in stagnation point, W/m<sup>2</sup>
q_c
\mathbf{R}
           control-effort weighing matrix
R
           radial distance,m
R_N
           nose radius, m
           activation (index 1) and de-activation (index 2) time of heat-flux tracking, s
           flight time, s
t_f
           control vector
\mathbf{u}
V
           velocity, m/s
V_c
           local circular velocity, m/s
           state vector
\mathbf{x}
           output vector
\mathbf{y}
           angle of attack, rad
\alpha
β
           angle of sideslip, rad
           flight-path angle, rad
\Delta...
           perturbed value
δ
           latitude, rad
ζ
           damping coefficient
           atmospheric density, kg/m<sup>3</sup>
ρ
\sum_{i}^{n}
           performance index
           bank angle, rad
\sigma
           longitude, rad
\tau
           heading, rad
\chi
           eigenfrequency, rad/s
\omega
           rotational rate of the Earth, rad/s
\omega_{cb}
```

I. Introduction

Satellites and other space vehicles that travel through the thicker layers of the atmosphere with high velocities are subject to large aerodynamic forces, and reach high temperatures as a result of aerodynamic heating due to friction. In general, these objects disintegrate and burn up completely, except for very large and very heavy parts. To safely reach the Earth's surface, accurate control over the trajectory is therefore mandatory. Moreover, to limit the mass of the vehicle's Thermal Protection System (TPS), an optimal trajectory that minimises the total integrated heat load should be flown. Also, to increase the number of reachable landing sites the vehicle should have maximum crossrange and downrange capabilities.

Minimising the integrated heat load can be achieved by flying at the maximum allowable heat flux, as this will greatly reduce the flight time and hence the thermal load. Tracking this heat-flux constraint in a robust manner is therefore key to a successful mission. However, the resulting trajectory will also induce relatively large mechanical loads, which should be constrained as well to avoid that the vehicle is getting damaged or worse yet, breaking up. Still, flying at the highest possible mechanical load is beneficial to reducing the integrated thermal load. Once a nominal trajectory fulfilling these so-called path constraints is available, it should be tracked accurately.

A straight-forward and simple implementation could be a (linear) output-feedback controller that has

a fast response, although its robustness could be doubtful due to insufficient damping. Designing such a tracking guidance is easy due to the well established design methodology using optimal-control theory, leading to a linear quadratic regulator using output weighing (LQY). A possible good alternative is a guidance-tracking system based on so-called simple adaptive control (SAC), which has shown a variety of applications in the field of, for instance, autopilot design² and entry systems. Such a system is known to have an excellent performance under the influence of rather large uncertainties, although its transient response could be sluggish at times. A potential problem, however, may be the large number of design parameters that can be tuned, without the existence of a proper design methodology.

Previous work focussed on setting up a rudimentary nominal guidance scheme for heat-flux tracking and analysed the implementation of the aforementioned tracking systems, as well as an integrated approach combining the two to check whether the strong points of the individual systems could be combined.^{4,5} Outcome of that study was that for a nominal mission the performance of the two individual tracking systems is equal. A Monte-Carlo analysis indicated that the tracking error is smaller for the output-feedback controller, but due to its longer tracking time the total heat load is smaller for the adaptive system. Integrating the two systems yielded a significant reduction of the tracking error, albeit at the expense of a larger guidance effort. However, the designs were sub-optimal to justify a proper conclusion.

The robustness of the nominal guidance system was improved in a follow-up study.⁵ Since the induced loads are sensitive to discrete changes in the guidance commands, particular attention was paid to a smooth transition between the two phases. Second, the output-feedback tracking system was extended to include the mechanical load and to avoid disruptions due to switching from one mode to the other. The next step in the ongoing research and the last extension of the fully integrated guidance system, *i.e.*, the addition of adaptive tracking, will be addressed in the current paper, in combination with an extensive robustness analysis of all components of the guidance system.

The layout of this paper is as follows. Section II will introduce the vehicle model and the equations of motion. In Section III, the guidance system is described, consisting of three parts: the nominal guidance, the inner-loop tracking system based on linear output feedback, and the outer-loop adaptive tracking guidance. In Sec. IV the performance of the nominal guidance system is analysed for a variety of entry conditions, tracking set points and vehicle mass. Section V presents the results of a more extensive analysis of the tracking systems under the influence of vehicle uncertainties and environmental perturbations. Section VI, finally, concludes this paper.

II. Model Description

A. Vehicle and Mission

The vehicle that we consider in the present study is a small, low-cost re-entry testbed for hypersonic experiments, designated *Hyperion-1*, and originally studied in the mid and late nineties.⁶ Purpose of this vehicle was to execute a wide range of experiments in hypersonic flight, otherwise not possible in ground-based facilities. Examples of such experiments are the testing of thermal-protection materials and coatings in a real-gas environment, aerodynamic measurements, such as boundary-layer transition and shockwave boundary-layer transition, and testing of new guidance, navigation and control (GNC) systems during re-entry. An example of the latter could be the path-constraint tracking system developed and discussed in this paper.

The re-entry module has a triangular shape with rounded corners and has three flaps mounted on the base for aerodynamic control during atmospheric flight (Fig. 1). In the current study, however, we consider the vehicle configuration without flaps; control could be achieved by reaction-control thrusters or moving masses, but this is not detailed here. The total vehicle mass is defined to be m=450 kg. The aerodynamic properties of the base vehicle are based on the assumption of modified Newtonian flow, by taking only pressure forces into account and neglecting skin friction.

A typical reference scenario for an entry (test) vehicle could be one that maximises its flight range while at the same time minimising the integrated heat load. Such a flight can be achieved by flying along a maximum heat-flux constraint as long as possible, since this will minimise the total flight time. This maximum heat flux should, of course, be within the capabilities of the vehicle's thermal protection system; to lower the peak heat flux, the flight is initiated at maximum angle of attack. Once the peak heat-flux has passed, the angle of attack may be lowered to a value that will maximise the lift-to-drag ratio, L/D, a condition that maximises the flight range.

An example of such a reference mission is shown in Fig. 2, starting from low Earth orbit (LEO) re-entry

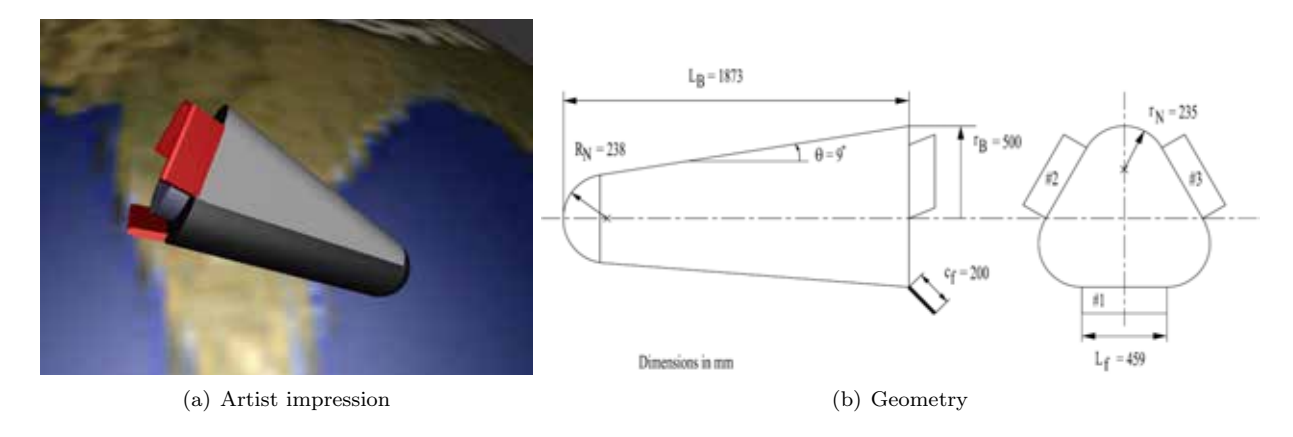


Figure 1. Hyperion-1 re-entry vehicle.⁶

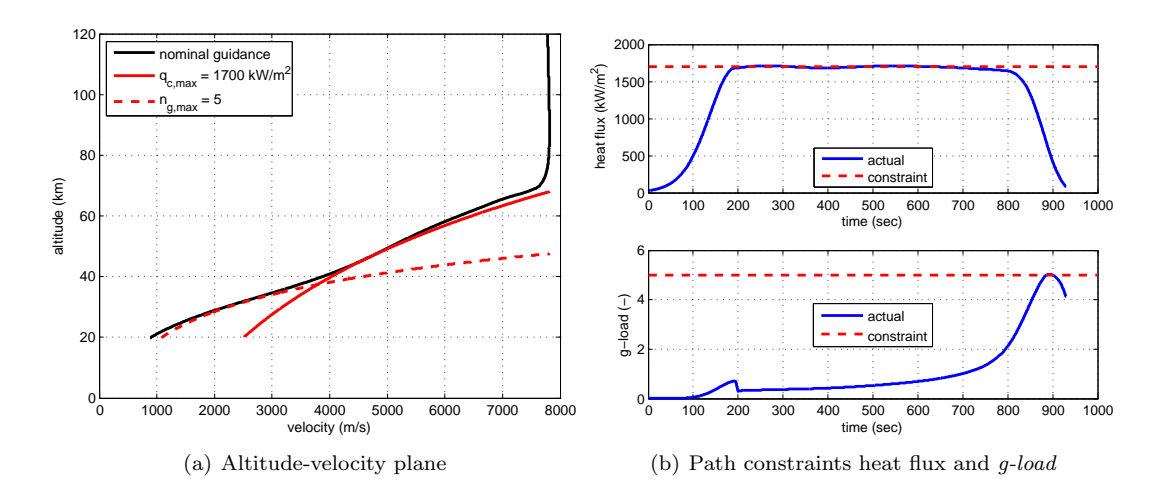


Figure 2. Typical Hyperion-1 reference trajectory.⁶

conditions, i.e., h=119.81 km, $\tau=-119.5^{\circ}$, $\delta=7.56^{\circ}$, V=7.782.5 m/s, $\gamma=-2.87^{\circ}$ and $\chi=90.18^{\circ}$. Besides the heat-flux constraint, also a maximum allowable mechanical load should be observed, as violating that constraint may lead to the destruction of the vehicle. From the plots, it is clear that Hyperion-1 flies along the two active path constraints heat flux and g-load, although the flight along the g-load constraint is only brief. The small deviations from the constraints are easily attributed to the simplifications that were made while setting up the trajectory design, which included, amongst others, a non-rotating Earth and an exponential density profile. The time histories of the two constraints confirm the correctness of the chosen trajectory design: the constraints are tracked well enough given the assumptions.

B. Flight Dynamics

The motion of re-entry vehicles is mainly driven by the combination of aerodynamic and gravitational forces and moments. Depending on the inherent non-linearities in the vehicle's aerodynamic characteristics, the extent of the flight regime under consideration, and asymmetry in the mass distribution of the vehicle, this motion can only be accurately described by a set of coupled first-order non-linear differential equations.

To describe the flight dynamics we use the position and velocity definition in spherical coordinates. This choice is primarily motivated by the fact to use the same model for the guidance-system development as well as simulating the flight dynamics. The position is defined by the distance $R = R_e + h$, longitude τ and latitude δ , whereas the velocity is expressed by its modulus, the groundspeed V, and two direction angles, *i.e.*, flight-path angle γ and heading χ . The attitude of the vehicle, or, in mathematical terms, the orientation of the body-fixed reference frame with respect to the trajectory reference frame, is expressed by the so-called aerodynamic angles, *i.e.*, the angle of attack α , the angle of sideslip β and the bank angle σ .

The dynamic equations of translational motion for a rotating, spherical Earth are given by ⁷

$$\dot{V} = -\frac{D}{m} - g\sin\gamma + \omega_{cb}^2 R\cos\delta(\sin\gamma\cos\delta - \cos\gamma\sin\delta\cos\chi) \tag{1}$$

$$\dot{\gamma} = \frac{L\cos\sigma}{mV} - \frac{g}{V}\cos\gamma + 2\omega_{cb}\cos\delta\sin\chi + \frac{V}{R}\cos\gamma + \omega_{cb}^2\frac{R}{V}\cos\delta(\cos\delta\cos\gamma + \sin\gamma\sin\delta\cos\chi)$$
 (2)

$$\dot{\chi} = \frac{L \sin \sigma}{mV \cos \gamma} + 2\omega_{cb}(\sin \delta - \cos \delta \tan \gamma \cos \chi) + \frac{V}{R} \cos \gamma \tan \delta \sin \chi + \omega_{cb}^2 \frac{R}{V \cos \gamma} \cos \delta \sin \delta \sin \chi \qquad (3)$$

whereas the kinematic position equations are given by

$$\dot{R} = \dot{h} = V \sin \gamma \tag{4}$$

$$\dot{\tau} = \frac{V \sin \chi \cos \gamma}{R \cos \delta} \tag{5}$$

$$\dot{\delta} = \frac{V\cos\chi\cos\gamma}{R} \tag{6}$$

In the above equations D and L are the aerodynamic drag and lift in N, g is the gravitational acceleration in m/s², and ω_{cb} is the rotational rate of the Earth in rad/s.

III. Guidance System

The guidance system for Hyperion consists of a nominal guidance that produces the reference commands (and thus a reference trajectory that meets with the path constraints heat flux and g-load), and a tracking system, which guarantees that the reference profile is followed as closely as possible. This tracking system consists of a so-called inner-loop and outer-loop component. The conceptual design of the guidance system is shown in Fig. 3, of which its basic design has been discussed in previous work.^{4,5}

The operational principle of the system is as follows. The mission manager provides the heat-flux and g-load set points (i.e., the constraint values) as well as relevant guidance-system parameters. Based on the flight condition (combination of altitude and velocity), the nominal guidance will determine the reference value for the bank angle using simplified models. The angle of attack is kept at a constant (maximum) value

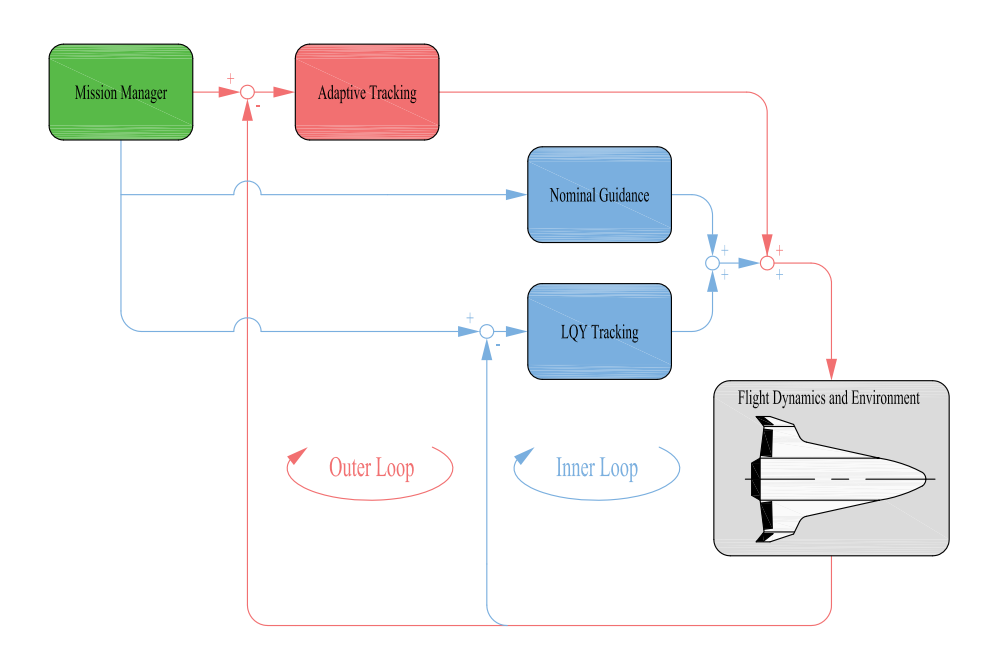


Figure 3. Integrated guidance system: nominal guidance plus LQY, and adaptive tracking guidance.

at the beginning of the flight, and will be lowered to provide maximum-range flight characteristics once the peak heat flux has been passed. Because of the assumptions made for the nominal guidance, the actual flown trajectory will deviate from the nominal one, and introduce errors in heat flux and/or g-load. These errors are initially removed by the LQY tracker – the inner-loop tracking. This loop is meant to stabilise the vehicle by using the fast response characteristics of the LQY. Both the nominal guidance and the LQY tracker will be discussed in more detail in Sec. III.A. Activation of the heat-flux tracking will only be done when the difference with respect to the set point is less than 10% to avoid saturation; for larger errors, the nominal guidance is expected to take care of that.

To try and improve the performance of the guidance system, *i.e.*, to reduce the tracking error as well as the guidance effort, an outer-loop adaptive guidance system is added. This outer loop, sampled at 50 Hz, aims to remove the remaining tracking error and provide additional robustness against disturbances, as the LQY is a linear output feedback controller that does not always handle non-linear effects well. The adaptive tracking system will be detailed in Sec. III.B.

A. Inner-Loop Guidance

1. Nominal Commands

Without trying to aim for a specific landing site, the objective of the nominal guidance is to combine the aspects of minimum heat load, which yields a minimum mass of the thermal-protection system, and maximum range that allows for more manoeuvrability towards a potential landing site. Since these two objectives are partly conflicting, the resulting trajectory will not be optimal in either objective, although a good compromise is reached that is suitable as nominal mission. A minimum heat-load trajectory is achieved by tracking the maximum allowable heat flux for as long as possible, as this will minimise the flight time, which has a dominating effect on lowering the heat load. The task of the nominal guidance is therefore to provide a bank-angle profile that ensures this; the angle of attack is initially commanded to a maximum value ($\alpha_{c,1} = 45^{\circ}$), to minimise the peak heat load early in the flight, and after passing this peak lowered to a value corresponding to a maximum lift-to-drag ratio that maximises the flight range ($\alpha_{c,2} = 20^{\circ}$). Finally, to avoid a too large mechanical load on the vehicle, a second path constraint on g-load is included in the nominal guidance. As will be explained, these path constraints can be combined in a single guidance law.

For the heat flux, q_c , the (cold-wall) Chapman model is used as a first approximation:

$$q_c = \frac{c_1}{\sqrt{R_N}} \sqrt{\frac{\rho}{\rho_0}} \left(\frac{V}{V_c}\right)^{c_2} = c^* \sqrt{\rho} V^{c_2}$$

$$\tag{7}$$

with $c_1 = 1.06584 \cdot 10^8$ W/m^{3/2}, $R_N = \text{nose radius} = 0.238$ m, $\rho = \text{atmospheric density (kg/m}^3)$, $\rho_0 = \text{density at sea level} = 1.225$ kg/m³, $V_c = \text{circular velocity at re-entry} = 7,905$ m/s, and $c_2 = 3$. A constraint value of $q_{c,max} = 1,700$ kW/m² is taken, which results in a stagnation-point temperature of about 2400 K. This heat-flux constraint will be elaborated upon at the end of this section.

The g-load, n_g , is defined to be the normalised acceleration due to the aerodynamic forces, i.e.,

$$n_g = \frac{\sqrt{D^2 + L^2}}{mq_0} = \frac{\sqrt{C_D^2 + C_L^2}}{mq_0} \rho V^2 S_{ref}$$
 (8)

where C_D and C_L are the drag and lift coefficient, S_{ref} is the aerodynamic reference area, m is the vehicle mass and $g_0 = 9.81 \text{ m/s}^2$ is the standard gravitational acceleration at the Earth's surface. A nominal constraint value of $n_{g,max} = 5$ is used in this study; this value may have to be re-evaluated at a later stage when more insight in the evolution of n_g is obtained.

With the assumption that C_D and C_L are Mach-independent during the hypersonic descent, the dynamic pressure is constant along the g-load constraint. As a result, the constraints have the following proportionality:

$$q_c = c_{q_c} \sqrt{\rho} V^3$$
 and $n_g = c_g \rho V^2$ (9)

with c_{qc} and c_g being the proportionality constants. By squaring the heat-flux constraint it becomes clear that both constraints can, in fact, be combined into a single expression in which ρV^n is constant, with n=6 for the heat flux and n=2 for the g-load. Using simplified equations of motion a guidance law using

bank-angle control to follow these path constraints can be derived. From the condition $\rho V^n = \text{constant}$ it follows that:

$$\frac{\mathrm{d}(\rho V^n)}{\mathrm{d}t} = \frac{\mathrm{d}\rho}{\mathrm{d}h}\dot{h}V^n + n\rho V^{n-1}\dot{V} = 0 \tag{10}$$

Assuming an exponential atmosphere and with Eqs. (4) and (1) substituted, while ignoring the small centrifugal-acceleration term in the latter, this results in:

$$-\frac{\rho}{H_s}V^{n+1}\sin\gamma - n\rho V^{n-1}\left(\frac{c_n}{2KV^{n-2}} - g\sin\gamma\right) = 0 \tag{11}$$

in which $K = \frac{m}{C_D S_{ref}}$ is the ballistic coefficient (kg/m²). Re-arranging terms yields for the "commanded" flight-path angle, γ_c , that fulfills the tracking criterion:

$$\sin \gamma_c = -c_n \frac{n}{V^{n-2}} \frac{H_s}{2K} \frac{1}{V^2 - naH_s} \tag{12}$$

with $c_n = \rho V^n$ = constant and $H_s = 7{,}050$ m being the scale height.

To link γ_c with the external forces, most notably the vertical lift force that is linked with the commanded bank angle, $\sigma_{0,c}$, the derivative of Eq. (12) with respect to velocity yields:

$$\frac{\mathrm{d}\gamma}{\mathrm{d}V}\bigg|_{c} = \frac{c_{n}}{\cos\gamma_{c}} \left\{ \frac{2n^{2}KH_{s}(V^{n-1} + gH_{s}(n-2)V^{n-3})}{[2KV^{n-2}(V^{2} + gnH_{s})]^{2}} \right\}$$
(13)

Because the time derivative of γ can be written as $\dot{\gamma} = \frac{\mathrm{d}\gamma}{\mathrm{d}V}\dot{V}$, the value of $\sigma_{0,c}$ can be found from the differential equations for γ , Eq. (2), and V, Eq. (1). The accelerations due to the rotation of the Earth are kept in the derivation to minimise the deviation from the actual flight path; in particular the Coriolis acceleration cannot be ignored.

$$V \left. \frac{\mathrm{d}\gamma}{\mathrm{d}t} \right|_{c} = \frac{L\cos\sigma_{0,c}}{m} + \sum (a_{\gamma})_{i} \tag{14}$$

with $\sum_{i} (a_{\gamma})_{i}$ being the sum of all acceleration terms other than the vertical-lift acceleration:

$$\sum_{i} (a_{\gamma})_{i} = -g \cos \gamma_{c} + 2\omega_{cb} V \cos \delta \sin \chi + \frac{V^{2}}{R} \cos \gamma_{c} + \omega_{cb}^{2} R \cos \delta (\cos \delta \cos \gamma_{c} + \sin \gamma_{c} \sin \delta \cos \chi)$$
 (15)

Isolating the bank angle yields:

$$\cos \sigma_{0,c} = \frac{m}{L} \left[\frac{\mathrm{d}\gamma}{\mathrm{d}t} \Big|_{c} - \sum_{i} (a_{\gamma})_{i} \right] = \frac{m}{L} \left[\frac{\mathrm{d}\gamma}{\mathrm{d}V} \Big|_{c} \dot{V} - \sum_{i} (a_{\gamma})_{i} \right]$$
(16)

The above guidance law assumes not only $\dot{\gamma}_c$, but also a reference value γ_c . The latter may be different from the actual γ , due to uncertainties in environment or vehicle characteristics, and to compensate for this difference a small correction term, $\Delta \dot{\gamma}_c$, may be added to $\dot{\gamma}_c$, given by Eq. (14). With $e_{\gamma} = \gamma_c - \gamma$ being the error in γ , a PID compensator in the form of

$$\Delta \dot{\gamma}_c = K_{\gamma p} e_{\gamma} + K_{\gamma i} \int_0^t e_{\gamma} dt + K_{\gamma d} \frac{\mathrm{d}e_{\gamma}}{\mathrm{d}t}$$
(17)

can serve that purpose. The gain values can easily be found by trial and error, or in a smarter way by specifying the (second-order) dynamics of the open-loop transfer function of the gamma-error to gamma-rate block, in the form of a damping, ζ_{γ} , and natural frequency, ω_{γ} . Using a PI regulator, it was found that for $\zeta_{\gamma} = 0.7$ and $\omega_{\gamma} = 3$ rad/s, the system was indeed functioning properly. These parameters correspond with the following gains: $K_{\gamma p} = 2\zeta_{\gamma}\omega_{\gamma} = 4.2 \,\mathrm{s}^{-1}$, $K_{\gamma i} = \omega_{\gamma}^2 = 9 \,\mathrm{s}^{-2}$. Furthermore, to provide more damping, a derivative gain $K_{\gamma d} = -0.1$ is selected after some trial and error, as it cannot follow from the open-loop analysis (three unknown gains from two known parameters). It is noted that a larger $K_{\gamma p}$ improves the transient response, but at the expense of noise amplification, leading to small-amplitude oscillations in σ_c .

At the transition from $q_c = \text{constant } n_g = \text{constant}$, at $t = t_{trans}$, a smooth transition of $\sigma_{c,0}$ should be modeled to avoid spikes in the guidance commands. A robust solution is to adapt the exponent n and to adjust the tracking constant ρV^n . So, during the transition from $n_1 = 6$ to $n_2 = 2$, triggered at a percentage f_{n_g} of $n_{g,max}^{\ a}$ an intermediate value for n is calculated according to a so-called *smooth* step function. Ken Perlin, in Ref. 8, suggests to use a fifth-order polynomial, which has zero 1st- and 2nd-order derivatives at x = 0 and x = 1: $f(x) = 6x^5 - 15x^4 + 10x^3$. With an argument n_x , normalised between 0 and 1, the smooth transition of n_g is then given by

$$n_x = \frac{n_g - f_{n_g} n_{g,max}}{n_{g,max} - f_{n_g} n_{g,max}} \tag{18}$$

$$n_{trans} = n_1 - (n_1 - n_2)n_x^3 \left(6n_x^2 - 15n_x + 10\right) \tag{19}$$

and the corresponding tracking constant

$$c_{n,trans} = \rho V^{n_{trans}} \tag{20}$$

For the first Δt_{trans} seconds in the transition phase, an extra smoothing to provide a seamless connection to the heat-flux tracking phase is applied^b:

$$t_x = 1 - \frac{\Delta t_{trans} - \Delta t}{\Delta t_{trans}}, \text{ with } \Delta t = t - t_{trans}$$
 (21)

$$c_{n,trans} = c_{n,q_c} - (c_{n,q_c} - \rho V^{n_{trans}})t_x^3 (6t_x^2 - 15t_x + 10)$$
(22)

A smooth transition is obtained with $\Delta t_{trans} = 15$ s. These values for n_{trans} , Eq. (19), and $c_{n,trans}$, Eq. (20) or Eq. (22), replace the corresponding values in Eq. (13), but other than that the algorithm remains the same.

Finally, the damping in case the tracking constant, c_n , changes rapidly, is improved with a simple PD regulator on the (normalised) tracking constant, *i.e.*,

$$\sigma_c = \sigma_{0,c} + K_{np} \frac{c_{n,act} - c_n}{c_n} + K_{nd} \frac{\dot{c}_{n,act}}{c_n} \tag{23}$$

where $\sigma_{0,c}$ is given by Eq. (16). Reasonable values for K_{np} and K_{nd} are -1 and -0.8, respectively, for the heat-flux phase, and $K_{np} = -1$ and $K_{nd} = -0.5$ for the *g-load*. In the transition phase, a smooth interpolation between the corresponding gain values is applied.

As an example of the performance of the nominal guidance, in Fig. 4 the heat flux, g-load, and corresponding commanded bank angle are shown for different heat-flux set points. The nominal setting for the heat-flux and g-load constraint are $q_{c,max} = 1,700 \text{ kW/m}^2$ and $n_{g,max} = 5$. The former has been selected in line with the limitations of the vehicle: given the nose radius, aerodynamic characteristics and initial conditions, this peak flux is, in fact, the maximum value it reaches given the lift coefficient at $\alpha = 45^{\circ}$. A lower angle of attack (and thus smaller lift coefficient) would lead to a larger peak heat flux, provided nothing else changes. This means that the moment this set point is reached, the tracking is activated. Note that the value for $n_{g,max}$ has been chosen as a representative value for this kind of vehicle, without further underlying motivation.

So, once the heat flux reaches its maximum and is about to go down again, tracking is activated and with bank-angle modulation the heat-flux set point is followed – approximately, due to the assumptions made in developing the guidance law. This may be corrected by a perturbation guidance, as will be discussed shortly. What will happen if the set point is chosen below or above the vehicle's capabilities? Lowering the set point to $q_{c,max} = 1,500 \text{ kW/m}^2$ gives rise to a significant "overshoot", due to the strong, negative heat-flux gradient induced by the vehicle's natural motion. After crossing the set point, the tracking cannot recover from that gradient very quickly, partially because the bank angle is saturated at 180° , a full "lift-down" orientation. Still, once the set point is reached, a more or less constant q_c is followed, even though the value is a bit too large. The main complication is that the translational dynamics is rather "slow", and changes in the trajectory take quite some time to be effectuated.

^aBecause the g-load increases rapidly towards the end of the flight, $f_{n_q} = 0.2$ is selected for a good performance.

^bSince the constant $c_{n,q_c} = c_{n=6}$ for the heat-flux phase is determined at phase initiation, there is some drift in this constant due to the analytical approximation. Therefore there will be a (small) discrete jump in the constant when it is re-evaluated at the beginning of the transition. This jump in the constant will otherwise lead to a jump in σ_c of about 1°.

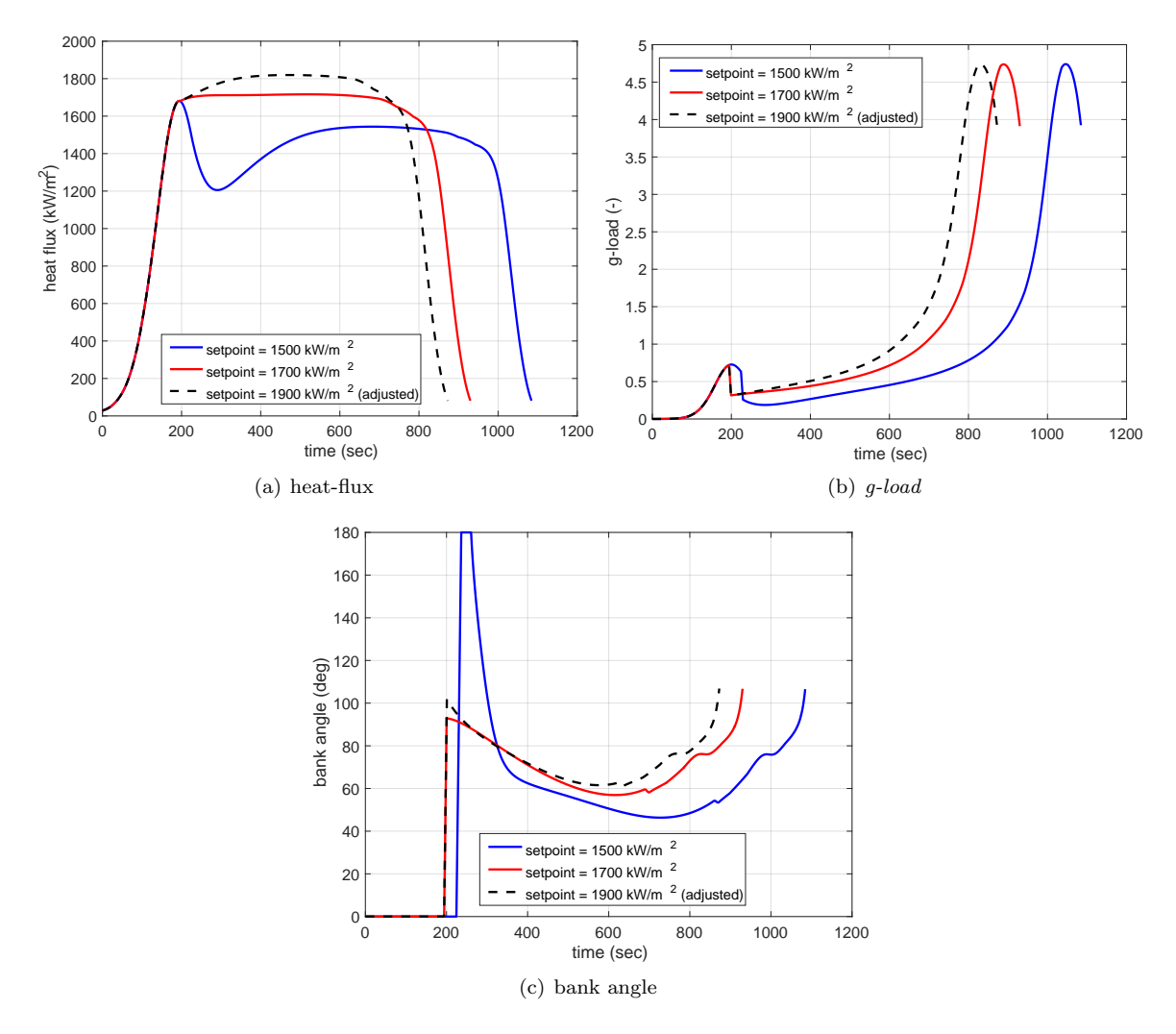


Figure 4. Nominal guidance for different heat-flux set points.

Increasing the set point to $q_{c,max} = 1,900 \text{ kW/m}^2$ did not do anything in the first implementation of the nominal guidance, because tracking was activated on the down-going flank of the heat flux. Since the peak value of the heat flux was below the set point, this maximum value was taken as tracking constant, resulting in exactly the same trajectory as if it was flown with $q_{c,max} = 1,700 \text{ kW/m}^2$. An important aspect to consider, though, is the fact that after crossing the moment of peak heat flux, the angle of attack is lowered to a value to maximise the flight range. Since for this α the lift coefficient is lower than the maximum value, this means that the heat flux could be increased. Therefore, the nominal guidance is adapted and the tracking constant is multiplied with a scaling factor, *i.e.*, the ratio between set point and the current maximum value – in this particular example 1,900/1,700. The effect is shown in the third curve of Fig. 4. It still takes some time, but indeed a larger value is being tracked.

It is noted that for all three trajectories the maximum g-load is not exceeded. This does not mean that this constraint is not "active". As mentioned before, the transition between heat-flux and g-load tracking is initiated at $n_g = 1$, so for a large portion of the flight the "n = 2"-tracking acts as a smooth interpolator. The maximum g-load is virtually the same for the three cases considered, and can be explained by the fact that when the heat flux starts reducing this is achieved by almost exactly the same bank-angle command history. Since the tracking constant is based on a combination of altitude and velocity, one might indeed expect that the trajectory shape is identical in the h-V diagram.

The remaining aspects of the nominal guidance to be discussed are the performance objectives and their relation to the variation in heat-flux setting. The objective functions heat load and maximum total range (i.e., the arc summation of down- and cross-range) are defined as follows. The heat load, Q, is simply

obtained by integrating the heat flux, Eq. (7):

$$Q = \int_{0}^{t_f} q_c dt \tag{24}$$

The total ground-track range, d_{total} , is calculated with the so-called Haversine function, which is historically used in navigation (the *haversine* is half the versed sine, *i.e.*, a flipped sine function with half the period). In this particular case the distance along the trajectory is integrated using spherical trigonometry. Given the position (τ, δ) at two time points t_i and t_{i+1} , the distance covered in the time interval $\Delta t = t_{i+1} - t_i$ is calculated with:

$$a_1 = \sin^2\left(\frac{\Delta\delta}{2}\right) + \cos\delta_i \cos\delta_{i+1} \sin^2\left(\frac{\Delta\tau}{2}\right)$$
 (25)

$$a_2 = 2\operatorname{atan}\left(\frac{\sqrt{a_1}}{\sqrt{1 - a_1}}\right) \tag{26}$$

$$d_{total} = R_e a_2 \tag{27}$$

with $\Delta \tau = \tau_{i+1} - \tau_i$ and $\Delta \delta = \delta_{i+1} - \delta_i$, and $R_e = \text{equatorial radius of the Earth} = 6,378.137 \text{ km}$.

For the three discussed set points, as well as two intermediate values, the resulting Q and d_{total} are listed in Table 1. A few observations. The higher the heat-flux set point, the smaller the integrated heat load, confirming that tracking the heat-flux constraint is indeed favouring the TPS design in terms of total mass. Total variation in Q is about 9%. Variation in flight range is more pronounced, *i.e.*, close to 20%. However, a gain in flight range is in conflict with lowering Q, so during the vehicle and mission design these two objectives need to be balanced.

Table 1. Nominal guidance for different heat-flux set points.

setpoint	Q	d_{total}
$\mathrm{kW/m^2}$	$\times 10^3 \mathrm{\ MJ/m^2}$	km
1,500	1,353.3	6,703.1
1,600	1,297.8	6,103.8
1,700	1,278.8	5,743.1
1,800(*)	1,250.9	5,541.6
1,900(*)	1,229.4	5,390.2

(*) scaled tracking constant

2. Tracking Commands

The inner-loop tracking guidance is based on output feedback, where the deviation from the nominal heat flux and/or maximum g-load is countered by a corrective bank-angle (and possibly angle-of-attack) command that affect the magnitude and orientation of the aerodynamic force components, D and L. The following guidance law defines this:

$$\Delta \mathbf{u} = -\mathbf{K_g} \Delta \mathbf{y} \tag{28}$$

where $\Delta \mathbf{y}$ is the deviation from the nominal output, yielding a corrective guidance command $\Delta \mathbf{u}$. The gain matrix $\mathbf{K_g}$ can be obtained by specifying the maximum output deviation $\Delta \mathbf{y}_{max}$ and control effort $\Delta \mathbf{u}_{max}$, and solving the optimal cost criterion for a linearised system:

$$\Delta \dot{\mathbf{x}} = \mathbf{A} \Delta \mathbf{x} + \mathbf{B} \Delta \mathbf{u} \qquad \Delta \mathbf{y} = \mathbf{C} \Delta \mathbf{x} \tag{29}$$

The resulting controller is known as a linear quadratic output regulator (LQY). It is noted that rather than using the states V, γ , and h for vertical motion, the flight-path angle and altitude are combined into a so-called pseudo altitude, h^* . Reason for doing so is that h is not directly controllable, only through a change in γ , so merging the two will give a more unified approach. So:

$$h^* = h + K_{\gamma}\gamma \tag{30}$$

where K_{γ} is a velocity-dependent gain, i.e., $K_{\gamma} = c_{\gamma}V$ m/rad; a value of $c_{\gamma} = 20$ s/rad is found to work well for this type of vehicle-mission combination.

Details about the design of this particular tracking system is provided in Refs. 4,5. There, the **A**, **B** and **C** matrices are shown for $\Delta \mathbf{x} = (\Delta V, \Delta h^*)^{\mathrm{T}}$, $\Delta u = \Delta \sigma$, and $\Delta \mathbf{y} = (\Delta q_c, \Delta n_g)^{\mathrm{T}}$. In addition, the applied weighing on outputs and controls to calculate $\mathbf{K_g}$ is provided there. Because only one constraint can be active at a particular time, this implies that there are two tracking systems working in parallel. As the corrective guidance commands will reduce the two path constraints in the same way, in case of conflict the larger output of the two serves as the actual command. This guidance command is initially only a correction to σ_c , whereas $\Delta \alpha_c$ is kept zero. When there is no margin left in σ_c , e.g., when the vehicle is flying with full lift-down, a limited, additional compensation can be achieved by correcting α_c , but this is currently not implemented.

Towards the end of the heat-flux tracking phase, there is a sudden decrease in q_c when the vehicle's aerodynamic characteristics no longer sustain the descent-rate requirements. It is also at this point in the trajectory that the g-load is rapidly increasing, see, for instance, Fig. 2. When the constraint is tracked too long, the g-load will spike and violate its constraint value, but activating the g-load tracking abruptly (and putting Δq_c to zero) will also produce a peak in σ_c . Therefore, a smooth reduction of the heat-flux error to zero is required that limits the g-load, and at the same time smoothly reduces heat-flux tracking. The solution is found once more in the use of the smooth step-function. Defining a maximum decay duration, Δt_{decay} , and starting a timer when the nominal guidance decides that heat-flux tracking should no longer be active, the time t_{decay} enters the step function to generate a scaling factor $k_q(t)$ that runs from 1 to 0:

$$k_q(t) = 6t_{decay}^5 - 15t_{decay}^4 + 10t_{decay}^3$$
 (31)

such that the heat-flux error entering the tracking system, either the LQY or the SAG discussed in the next Sec. III.B, becomes:

$$\Delta q_c^* = k_q(t)\Delta q_c \tag{32}$$

A value of $\Delta t_{decay} = 10$ s has been found to work well.

The impact of applying a tracking system is shown in Fig. 5 for the nominal tracking constants of $q_{c,max} = 1,700 \text{ kW/m}^2$ and $n_{g,max} = 5$. It may be clear that the heat flux is better tracked and also for a longer time, although the effect on the objectives is not so pronounced. A slightly lower (= better) Q (1,269 versus 1,279 × 10³ MJ/m²) at the expense of a lower (= worse) d_{total} (5,697 versus 5,743 km). However, the benefit of the tracking guidance is not just to improve the nominal performance, but making it more robust against perturbations. This will be studied in more detail in Sec. V. For the sake of completeness, the other set points of Table 1 have been run with the tracking guidance as well. The results are listed in Table 2. For an easy comparison, both tables are visualised in Fig. 7. For low set points, the objectives are the same, as the tracking systems has to make the same effort as the nominal guidance to bring the vehicle to the "lower-than-natural" value. For larger set points, the tracking system improves on Q at the expense of d_{total} , as heat-flux tracking is the active constraint, whereas the flight range is more of a consequence of selecting $\alpha_{c,2}$ and the total flight time.

B. Outer-Loop Adaptive Output Tracking

The advantage of the LQY tracking system is that it can relatively quickly remove errors close to its design trajectory. A potential drawback may be be that in case there are persistent perturbations, either originating from the environment or the vehicle,

The outer-loop tracking guidance is based on so-called simple adaptive control (SAC), and is based on the concept of tracking the output of a reference model. Such a control scheme is part of the larger class of model reference adaptive control (MRAC). In line with the designation of SAC, the developed adaptive tracking system will be referred to as simple adaptive guidance (SAG). The operating principle of a simple adaptive controller has been schematically depicted in Fig. 8. The tracking-guidance law is given by

^cWith the LQY, a combined $\Delta \alpha_c$ and $\Delta \sigma_c$ could be calculated; however, this would mean that the system is a single-input, dual-output system that – in a non-linear system – could potentially give rise to oscillations. Therefore, a single-input, single-output (SISO) tracking system is preferred.

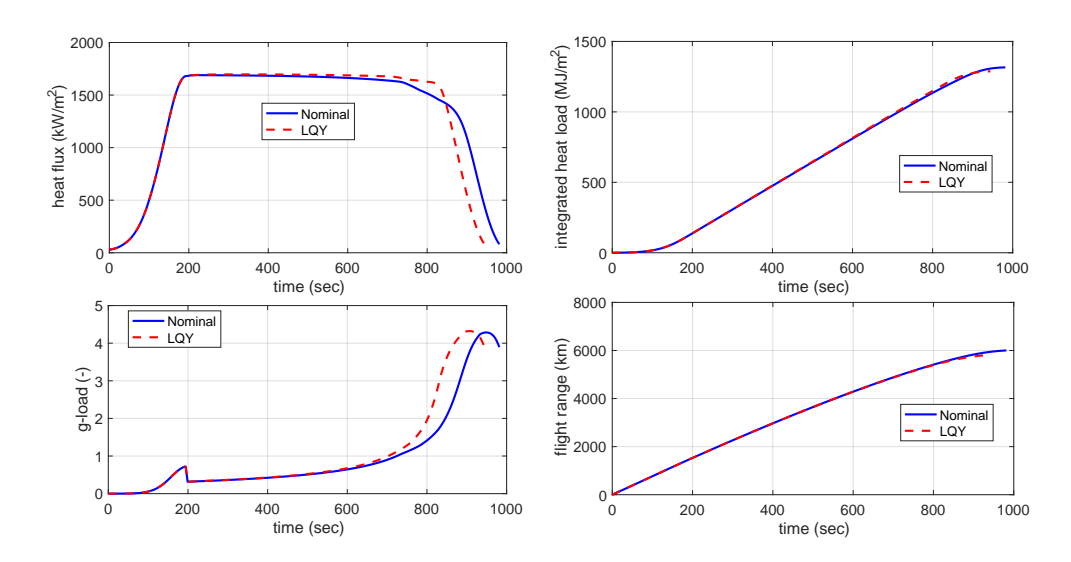
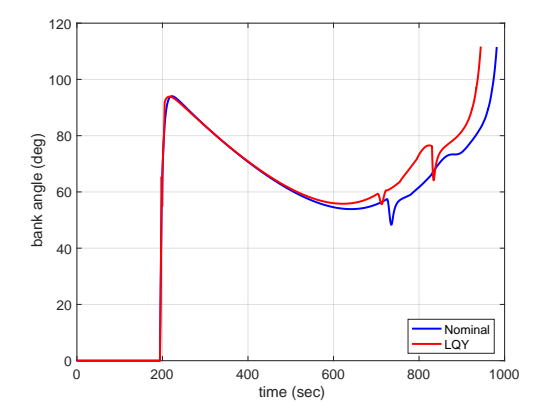


Figure 5. Nominal mission performance: Nominal guidance versus LQY tracking.

Table 2. Tracking guidance for different heat-flux set points.

setpoint	Q	d_{total}
${ m kW/m^2}$	$\times 10^3 \mathrm{\ MJ/m^2}$	km
1,500	1,353.8	6,724.5
1,600	1,295.0	6,099.5
1,700	1,268.8	5,696.5
1,800	1,215.8	5,316.2
1,900	1,170.7	5,012.2



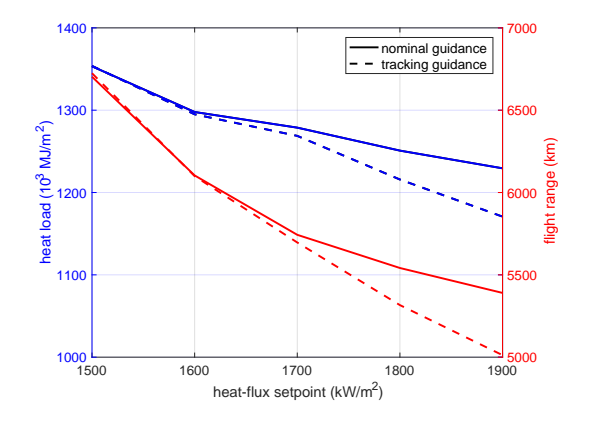


Figure 6. Nominal mission performance: bankangle profile.

Figure 7. Integrated heat load and total flight range as a function of maximum heat-flux set point.

$$\Delta \mathbf{u}(t) = \mathbf{K_r}(t)\mathbf{r}(t) \tag{33}$$

where $\mathbf{r}(t) = [\mathbf{e_y}(t) \ \mathbf{x_m}(t) \ \mathbf{u_m}]^T$ and $\mathbf{K_r}(t) = [\mathbf{K_e}(t) \ \mathbf{K_x}(t) \ \mathbf{K_u}(t)]$. It can be seen that the model input $\mathbf{u_m}$ and model state $\mathbf{x_m}$ are required to form part of the input signal $\mathbf{u_p}$ to the plant. Moreover, the so-called output error $\mathbf{e_y}$ serves as a feedback quantity to form the third element that composes $\mathbf{u_p}$. The three gains, *i.e.*, $\mathbf{K_x}$, $\mathbf{K_u}$ and $\mathbf{K_e}$, are adaptive. The weighting matrices $\mathbf{T_p}$ and $\mathbf{T_i}$ are positive semi-definite and positive definite, respectively.

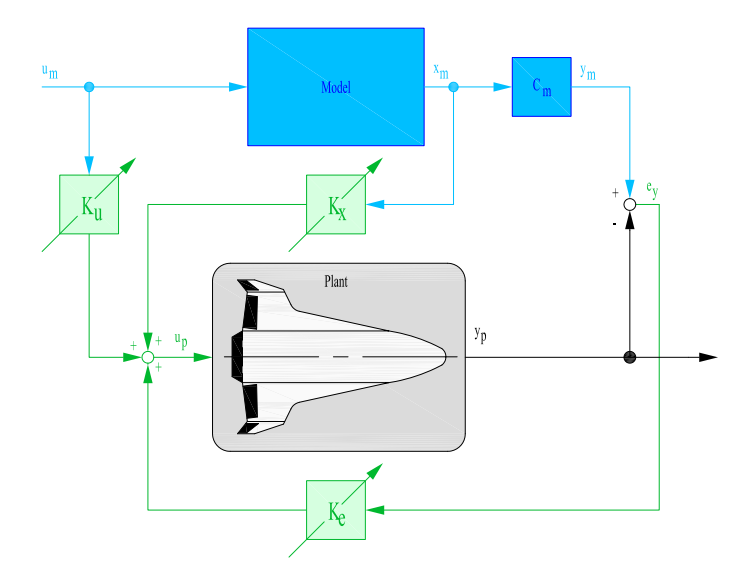


Figure 8. Basic architecture of a Simple Adaptive Control algorithm.

To compute the adaptive gains, $\mathbf{K_r}$ is defined to be the sum of an integral and a proportional component:

$$\mathbf{K}_r(t) = \mathbf{K}_i(t) + \mathbf{K}_n(t) \tag{34}$$

with

$$\dot{\mathbf{K}}_{\mathbf{i}}(t) = \mathbf{e}_{\mathbf{y}} \mathbf{r}^{\mathrm{T}}(t) \mathbf{T}_{\mathbf{i}} \tag{35}$$

$$\mathbf{K}_{\mathbf{p}}(t) = \mathbf{e}_{\mathbf{y}}(t)\mathbf{r}^{\mathrm{T}}(t)\mathbf{T}_{\mathbf{p}} \tag{36}$$

Note that the proportional-gain component has a direct influence on the transient tracking behaviour, but is strictly speaking not required to enforce asymptotic tracking. This is guaranteed by the integral gain. To improve the transient response by only using an integral gain, a constant gain value can be added to $\mathbf{K_i}$. An advantage over the use of the proportional gain is that this constant value is independent of $\mathbf{e_y}$, and is therefore non-zero even if $\mathbf{e_y}$ is zero. In that case, the integral gain derived from Eq. (35) becomes

$$\mathbf{K_i}(t) = \mathbf{K_{i,0}} + \int_0^t \dot{\mathbf{K}_i}(t)dt$$
(37)

One way to improve the damping of the system is to include the error derivatives in the output error vector. In that case, the error for output \mathbf{y} becomes:

$$\mathbf{e}_{\mathbf{y}}(t) = \mathbf{K}_{\mathbf{y}}^{\mathrm{T}}(\mathbf{y}_{\mathbf{m}}(t) - \mathbf{y}_{\mathbf{p}}(t)) + \mathbf{K}_{\dot{\mathbf{y}}}^{\mathrm{T}}(\dot{\mathbf{y}}_{\mathbf{m}}(t) - \dot{\mathbf{y}}_{\mathbf{p}}(t))$$
(38)

with $\mathbf{K}_{\mathbf{y}}^{\mathrm{T}}$ and $\mathbf{K}_{\mathbf{y}}^{\mathrm{T}}$ being a proportional and derivative output gain, respectively. However, to avoid calculating the numerical derivative of the outputs and to tune the related gains in multiple-output systems an alternative expression for the output error is used. Adjusting the output matrix by pre-multiplying it with $\mathbf{K}_{\mathbf{g}}$, the optimal gain matrix from solving the Algebraic Riccati Equation, sufficient damping is introduced in the system to have a proper response. The output error becomes in that case

$$\mathbf{e}_{\mathbf{v}} = \mathbf{y}_{\mathbf{m}} - \mathbf{y}_{\mathbf{p}} = \mathbf{K}_{\mathbf{g}} \left(\mathbf{C}_{\mathbf{m}} \mathbf{x}_{\mathbf{m}}(t) - \mathbf{C}_{\mathbf{p}}(\mathbf{x}_{\mathbf{p}}, t) \mathbf{x}_{\mathbf{p}}(t) \right)$$
(39)

However, for a single-output system we use the simpler alternative^d, namely to add the derivative error term:

^dSimilarly to the design of the LQY tracking system, also the adaptive guidance has two individual components, *i.e.*, one for tracking the heat flux, and the other one for tracking the *g-load*. Both systems are single-input, single output systems, where the allocation to $\Delta \alpha_c$ and $\Delta \sigma_c$ is done outside the tracking systems.

$$e_{q_c}^* = e_{q_c} + K_{D,q_c} \dot{e}_{q_c}$$
 $e_{n_g}^* = e_{n_g} + K_{D,n_g} \dot{e}_{n_g}$ (40)

So far, an ideal environment has been considered. To cope with environmental disturbances that lead to a persistent non-zero error and therefore to a continuous change in the integral gain K_i , a robust design can be applied to adjust the integral gain and preventing it from reaching very high values. The integral term of Eq. (35) is adjusted as follows:

$$\dot{\mathbf{K}}_{\mathbf{i}} = \mathbf{e}_{\mathbf{v}}(t)\mathbf{r}^{\mathrm{T}}\mathbf{T}_{\mathbf{i}} - \sigma_{i}\mathbf{K}_{\mathbf{i}}(t) \tag{41}$$

Without the σ_i -term, $\mathbf{K_i}(t)$ is a perfect integrator and may steadily increase (and even diverge) whenever perfect output following is not possible. Including the σ_i -term, $\mathbf{K_i}(t)$ is obtained from a first-order filtering of $\mathbf{e_v}(t)\mathbf{r}^{\mathrm{T}}\mathbf{T_i}$ and, therefore, cannot diverge, unless the output error diverges.

Previously, the reference model was similar to the linearised model used to calculate the LQY gains, $\mathbf{K_g}$, *i.e.*, the state-space model given by $\mathbf{A_m}$, $\mathbf{B_m}$ and $\mathbf{C_m}$ and stabilised by an output-feedback guidance law.^{4,5} For the actual implementation it was found that during the heat-flux tracking phase the $\mathbf{A_m}$, $\mathbf{B_m}$ and $\mathbf{C_m}$ matrices (so also $\mathbf{K_m}$) are almost constant. The same can be said for the phase where the *g-load* needs to be observed, typically close to the end of the hypersonic descent. For ease of implementation a constant reference model for either phase can thus be considered. To have a representative model behaviour, the reference model was excited by the actual heat-flux error, *i.e.*, the difference between plant output (the actual heat flux) and the set point. This means, though, that the reference model becomes part of the feedback loop, which is not commonly done. It means that in the presence of a persistent output error or an underperformance of the non-linear plant both model state and model input can become quite large. The potential danger is that the plant input saturates, which may lead to loss of control.

The alternative would be to remove the model all together, as there is no obvious way to form an input signal to the model, representative for the problem at hand. This would mean that for a (constant) set-point tracking the adaptive guidance is driven by the output error only. For lack of a proper reference model, this implementation will thus be considered. The next choice is the one of guidance command. From theory it is known that to apply SAC and guarantee asymptotic stability the non-linear system should be almost strictly passive. For practical purposes, this means that to start with the system should have as many outputs as inputs. In other words, while tracking either a heat-flux or a g-load error (input), only one guidance command can be used (output). Preliminary analysis shows that angle-of-attack control is not as efficient in terms of tracking as bank-angle control. Summarised, this means that as baseline, a tracking system without reference model and bank-angle control is selected.

The tuning of the input parameters is done relatively $ad\ hoc$ and has led to the values listed in Table 3. The guidance system is sampled at a frequency of 50 Hz. It is stressed that with proper design-parameter tuning the performance can probably be improved, but for the current state of the research this is not pursued. Besides the mentioned parameters, the output-error derivative gains (Eq. (40)) are $K_{D,q_c}=9$ and $K_{D,n_g}=0$, with e_{q_c} and e_{n_g} being scaled with the corresponding LQY gains. The error derivative is calculated with backward differencing.

Table 3. Sub-optimal SAG parameters for output-error control.

element	T_p	T_i	$K_{i,0}$	σ_i
e_{q_c}	5	50	0.2	0.1
e_{n_g}	40	10	0.1	0.1

IV. Nominal Guidance

In Sec. III.A the performance of the nominal guidance was discussed for varying settings of the heatflux tracking set point. In this section the performance of the nominal guidance is further explored, both as a standalone system and in combination with the LQY tracking (inner-loop guidance), and also the combination of nominal guidance with the SAG (potential alternative inner-loop guidance). To do so, a Monte Carlo analysis is performed on mission-operational aspects, *i.e.*, the initial conditions, V_0 and γ_0 , the set points $q_{c,max}$ and $n_{g,max}$, the initial angle of attack for maximum lift and the one for maximum L/D,

Table 4. Settings for Monte-Carlo analysis nominal guidance.

variable	nominal value	range
$V_0 \text{ (m/s)}$	7,782.5	± 100
γ_0 (°)	-2.87	± 0.1
, - ()		
$q_{c,max} (kW/m^2)$	1,700	± 100
$n_{g,max}$ (-)	4.8	± 0.5
$\alpha_{c,1}$ (°)	45	± 2.5
$\alpha_{c,2} \ (^{\circ})$	20	± 2.5
m (kg)	450	±50

 $\alpha_{c,1}$ and $\alpha_{c,2}$, as well as the vehicle mass, m. These seven parameters are varied with the settings given in Table 4, according to a uniform distribution. A total of 200 simulations are executed, with all three batches following the same random sequence of the parameters to allow for a fair comparison.

It is noted that in anticipation of the sensitivity analysis in the next section, $n_{g,max}$ has been lowered from 5 to 4.8 to avoid (large) overshoots. The peak g-load is reached towards the end of the flight, when the tracking system tries to keep following the heat-flux and there is a strong gradient in g-load. Furthermore, the time for transition from $q_c = \text{const.}$ to $n_g = \text{const.}$ has been increased from $\Delta t_{trans} = 15$ s to 25 s.

To study the performance the two performance objectives, Q and d_{total} , are considered, as well as the maximum values occurring values of q_c and n_g . The results for the three batches are combined in Figs. 9 and 10. The integrated heat load shows a large variation, from 950 to $1,750 \times 10^3 \text{ MJ/m}^2$, where it can be seen that the tracking systems lower the Q and shift the mean towards the left in the figure. Both tracking systems seem to perform more or less equally well. The flight range varies between 4,300 and 8,400 km, with a negative effect of the tracking systems, *i.e.*, d_{total} is lower than the range for just the nominal guidance. Plotting d_{total} versus Q shows a similar pattern as seen in Fig. 7, so from this so-called Pareto front one can read the induced Q given the (required) flight range. Of course a more detailed analysis would be required to use this in actual mission design, but given all random variations of the input the relation between the two is quite clear.

To judge how well robust the nominal guidance is, given the variation in operational aspects and vehicle mass, Fig. 10 provides the maximum heat flux and maximum g-load that occur during the mission. As explained before, the nominal peak heat flux is determined by the entry conditions and the vehicle's aero-dynamic performance, and for given conditions the peak heat flux is just a consequence. However, from this

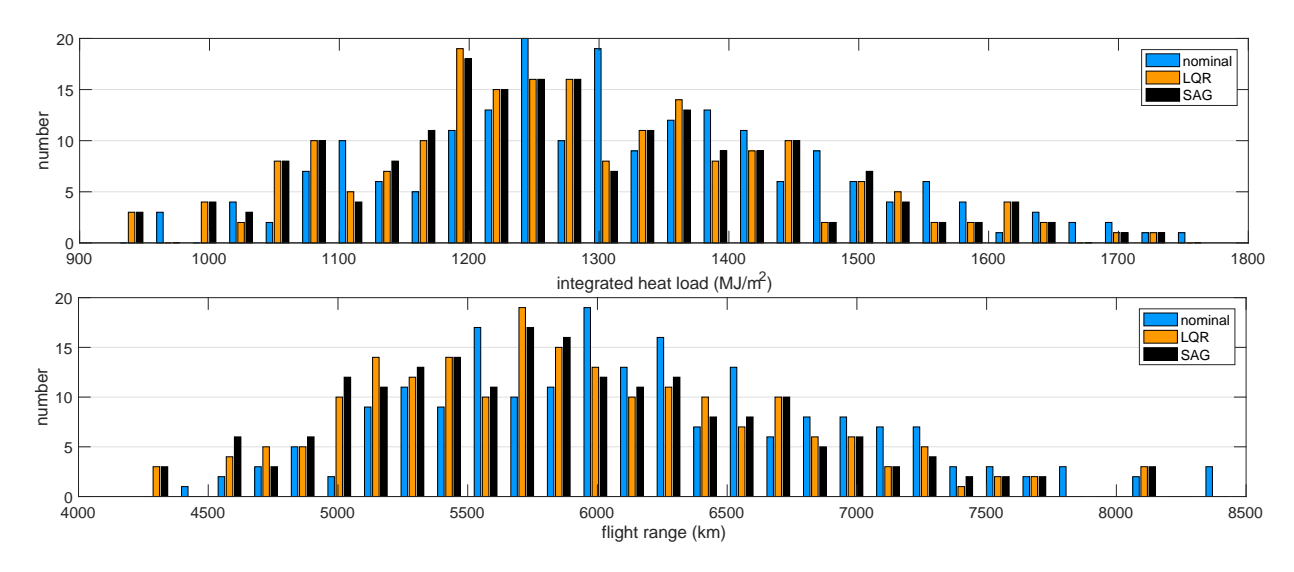


Figure 9. Integrated heat load and total flight range for various operational aspects (nominal-guidance performance).

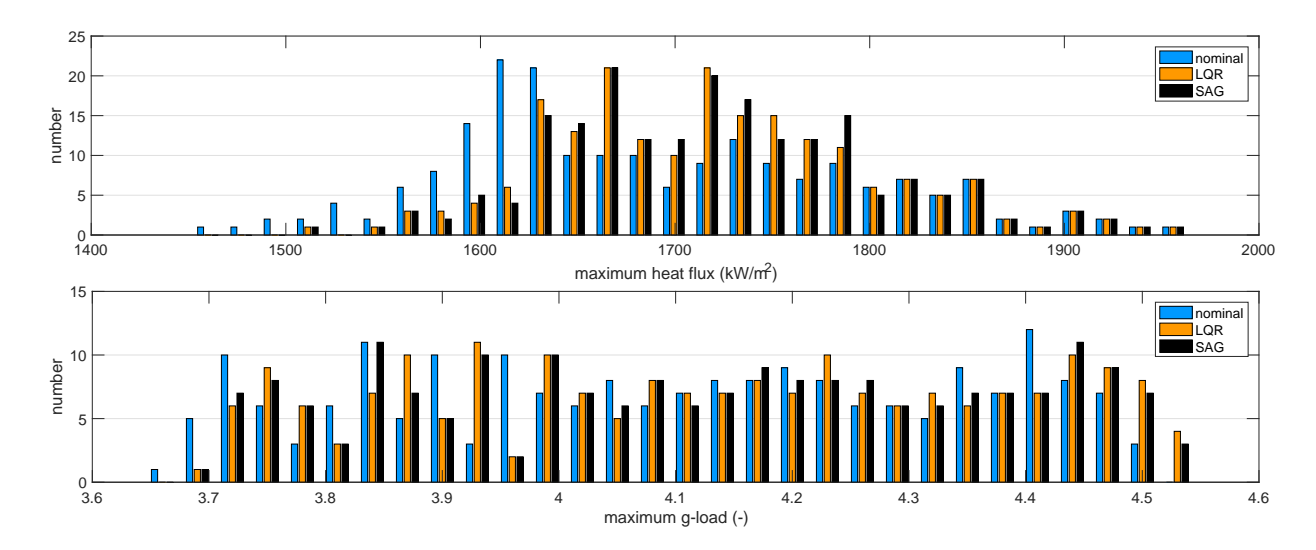


Figure 10. Maximum heat flux and g-load for various operational aspects (nominal-guidance performance).

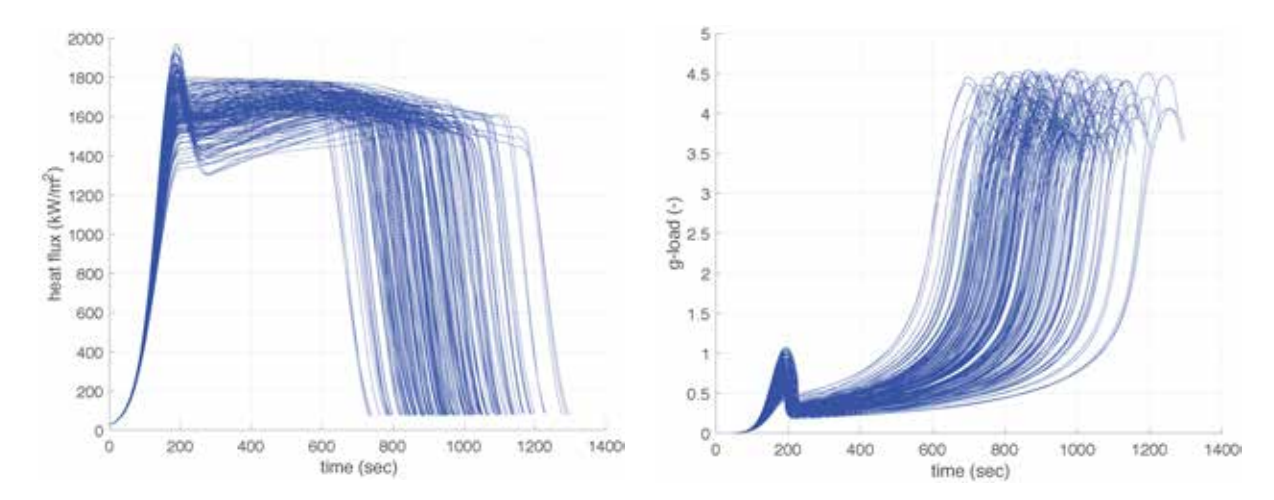


Figure 11. Time history of heat flux for nominal guidance with LQR tracking (200 runs).

Figure 12. Time history of gload for nominal guidance with LQR tracking (200 runs).

figure it can be concluded that there are no excessively large peak values, which means that in all cases the guidance system is stable and can thus be called robust with respect to the input variations. The heat-flux set point ranges from 1,600 to 1,800 kW/m², whereas the observed range is between 1,450 and 1,950 kW/m², an undershoot and overshoot of 150 kW/m². Because of active tracking the vehicle will move a bit faster towards the set point than with only the nominal guidance, hence the shift of the nominal-guidance data towards the lower end. However, the very low end is caused by limitations in the nominal guidance to actually track low set points. In that sense does the tracking help to narrow down the variation. The maximum g-load ranges from 3.65 to 4.55, which is very well acceptable. From this graph it is not clear whether a single run would have had a lower set point than the corresponding maximum value, but inspecting the individual runs confirms that there has not been any constraint violation.

To conclude the discussion on the nominal guidance, in Figs. 11 and 12 all individual curves of heat flux and *g-load* have been plotted. These figures confirm that the nominal guidance with LQR tracking operates well and gives a consistent performance under varying conditions. In the next section, the performance of the nominal inner-loop guidance, as well as the combination of inner-loop and outer-loop guidance will be analysed in case there are external perturbations.

V. Sensitivity Analysis

A. Approach

Until now, the performance improvements of the nominal guidance and the LQY tracking have been presented. In the current section the results of a sensitivity analysis will be discussed. The performance of the tracking system is judged using several performance indices. The first one is the integrated heat load, Q, which should be as low as possible to minimise the mass of the thermal protection system. Because this is achieved by flying along the heat-flux constraint, the second performance index is the integrated heat-flux deviation from this constraint. Mathematically this index is defined as

$$\sum_{q_{c,err}} = \int_{t_1}^{t_2} \sqrt{(q_c - q_{c,max})^2} dt$$
 (42)

with t_1 and t_2 the activation and de-activation time of the heat-flux tracking. This index has been visualised in Fig. 13(a), where the shaded area corresponds with Eq. (42). For the *g*-load tracking it is sufficient to integrate only the overshoots, because having a *g*-load smaller than $n_{g,max}$ should not be penalised. Thus, the third performance index is:

$$\sum_{n_{g,err}} = \int_{0}^{t} (n_g - n_{g,max}) \, dt, \, \forall \, n_g > n_{g,max}$$
 (43)

The corresponding guidance effort can be represented by the integrated bank angle over time, see Fig. 13(b). Here, the total guidance effort is considered, *i.e.*, the summation of nominal and tracking command, because the nominal guidance command is in principle affected by the tracking and should therefore be taken into account. The index is thus defined as:

$$\sum_{\sigma} = \int_{0}^{t_{final}} \sigma_c dt \tag{44}$$

It is obvious that these metrics should all be as small as possible. Note that since σ_c is always positive (lateral guidance is not considered), there is no need to take the absolute value. Other parameters of interest are the final flight time, t_f , as possible indicator why Q is large or not, and the maximum overshoot values of q_c and n_g . The extent to which these constraints are overshot gives an indication that thermo-mechanical

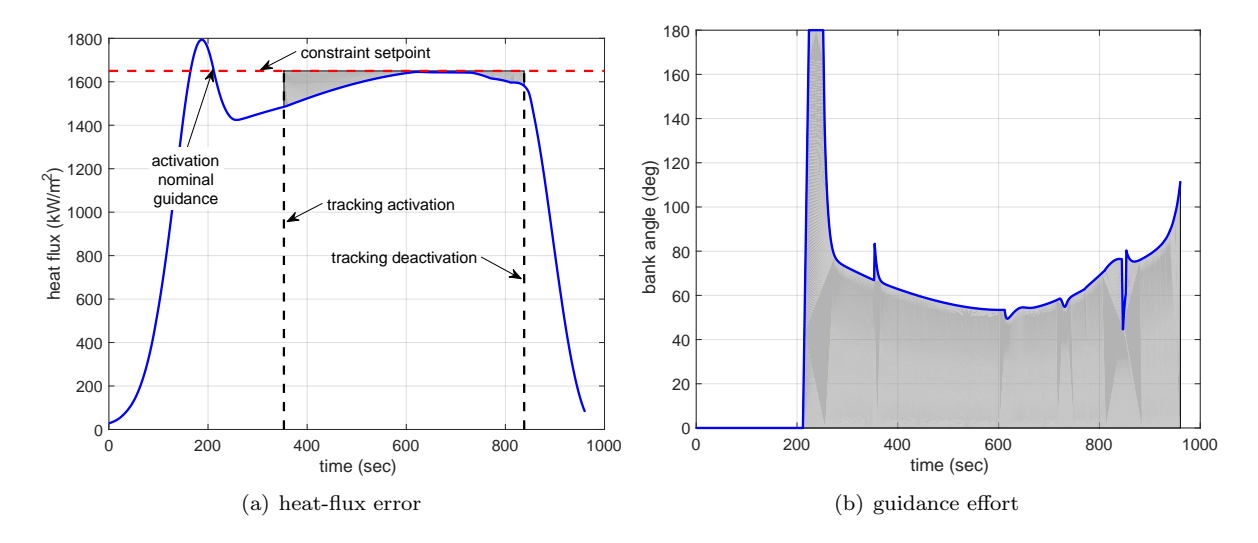


Figure 13. Integrated performance indices, represented by the shaded areas.

failure may be expected. A very large overshoot for only a short time may still lead to failure, even if the integrated constraint violation is small.

For the example shown in Fig. 13, the numerical values are: $\sum_{q_{c,err}} = 23.8$ MJ and $\sum_{\sigma_c} = 52,766.0$ °s. The reader is reminded of the fact that the tracking guidance is activated after initiation of the nominal guidance,

and when the difference with the heat-flux set point is less than 10%. This is done to avoid saturation of the tracking when the error is very large.

B. Results

As a baseline, the performance of both individual tracking systems (LQY and SAG), as well as the integrated system with an inner and outer loop, is compared for the nominal mission (Fig. 2), where corrective commands in σ_c are considered on top of the nominal profile. The performance is judged from the q_c and n_g profiles, as well as the guidance objectives to minimise Q and to maximise d_{total} . The LQY profiles have been shown earlier in Figs. 5 and 6, and the ones for the SAG and integrated tracking system are similar to those, and will therefore not be shown. However, the performance indices for each one of them are listed in Table 5. The results show that the LQY and SAG tracking work equally well, individually, with a slightly better performance for the SAG in terms of tracking error and guidance effort. However, the tighter control results in a slightly smaller flight range. Combination of the two tracking systems, though, gives a very tight heat-flux control at less guidance effort. The maximum heat flux is exactly the set point. The tighter control does increase the maximum g-load a bit and reduces d_{total} by about 100 km (less than 2%).

tracking	Q	d_{total}	$q_{c,max}$	$n_{g,max}$	$\sum_{q_{c,err}}$	\sum_{σ}
system	$\times~10^3~\mathrm{MJ/m^2}$	$\rm km$	${\rm kW/m^2}$	-	${ m MJ/m^2}$	\times 10 ³ °s
LQY	1,290.2	5,833.1	1,696.6	4.15	10.80	53.1
SAG	1,286.9	5,810.8	1,698.9	4.15	7.98	53.0
INT	$1,\!274.4$	5,734.8	1,700.0	4.46	1.60	52.1

Table 5. Performance indices for nominal mission.

Having established a baseline, all three tracking systems are now subjected to a number of environmental perturbations and vehicle uncertainties. For the combination of nominal guidance and LQY (or SAG) tracking, as well as the integrated system, a Monte-Carlo analysis consisting of 250 samples is executed with the variations in vehicle mass, $\Delta m = \pm 20$ kg, atmospheric density, $\Delta \rho = \pm 15\%$, speed of sound, $\Delta a = \pm 10\%$, and drag and lift coefficient, $\Delta C_D = \Delta C_L = \pm 10\%$. Each of the errors will be sampled from a uniform distribution with an identical random sequence for the perturbations for each batch. Even though no navigation system has been implemented, the guidance system uses nominal values of C_D , C_L , ρ (and thus \bar{q}), and a (and thus the Mach number, M), rather than the perturbed values. The only exception is the feedback value of q_c , which is assumed to be coming from ideal measurements. Anticipating on the sensitivity to the perturbations, the "smoothing" duration when initiating the transition between heat-flux and g-load tracking Δt_{trans} has been increased from 15 to 25 s. The results are shown in Figs. 14 through 16.

The results show a similar pattern as for the nominal mission: the LQY and SAG perform similarly, with the SAG being slightly better in terms of heat-flux tracking (and thus Q) with a smaller guidance effort. Of course, the flight range has degraded a bit as a result. The variation of the maximum heat flux is also smaller for the SAG, which indicates a tighter control. There are a few outliers with $\pm 80 \text{ kW/m}^2$, but on a nominal value of $q_{c,max} = 1,700 \text{ kW/m}^2$ this is less than 5%. The maximum g-load is well below the set point of 4.8 in all cases, ranging from about 4 to 4.5 g.

When the integrated tracking system is used, the integrated heat load goes down even more. However, the tighter tracking causes a significant variation in d_{total} between 5,100 and 6,500 km. As mentioned earlier, once a target flight range is specified a dedicated optimisation should relax the heat-flux tracking capability a bit such that the flight range can be met. Also the maximum g-load increases and ranges from 4.2 to almost 4.8 g. Tracking the heat flux for a longer time close to the descending leg towards the end of the flight has a consequence that the gradient of n_g is large, and may potentially lead to overshoot of the g-load constraint. This situation should be avoided, of course, and more analysis has to be done to find a robust solution. We

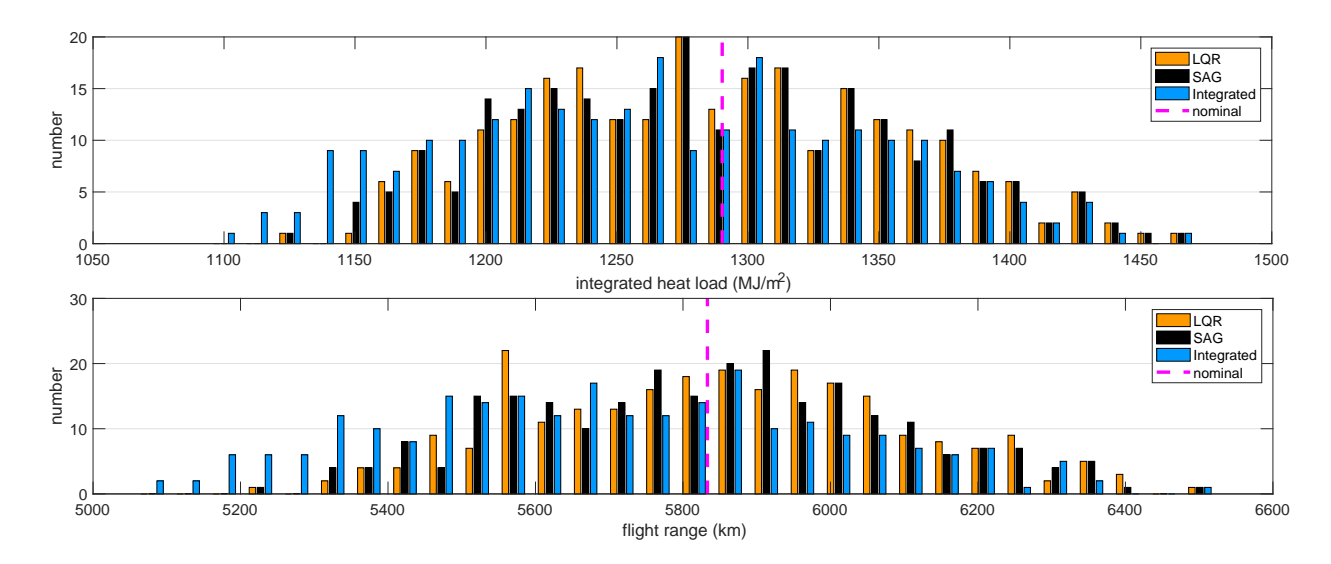


Figure 14. Integrated heat load and total flight range for sensitivity analysis (250 runs).

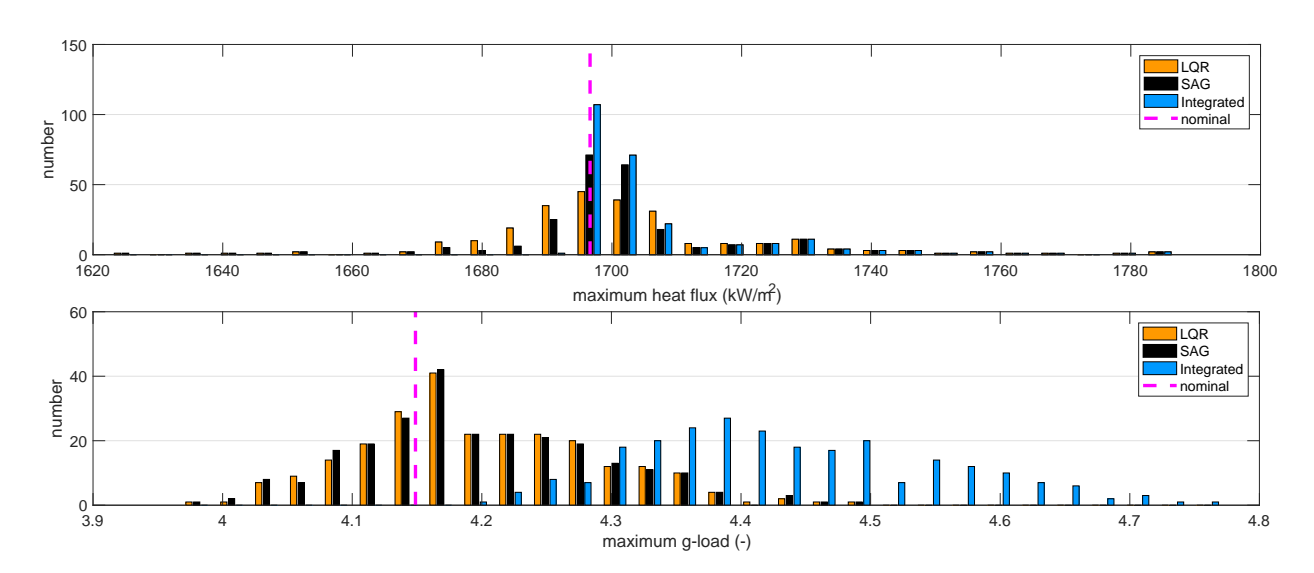


Figure 15. Maximum heat flux and g-load for sensitivity analysis (250 runs).

will briefly address this with a second batch of Monte Carlo runs with larger perturbations to find out the behaviour of the guidance system. A surprising observation in Fig. 16 seems to be that despite the tighter heat-flux tracking this requires less guidance effort for the integrated system. However, this performance index is indicative only and inspection of the local behaviour of σ_c should be included in future analyses.

As mentioned, a second Monte-Carlo batch will be executed to test the limits of the guidance system. This will be done only for the integrated system, as this system gave the best results, but may also the most susceptible to g-load-constraint violation. The applied uncertainties that are taken into account are the vehicle mass (± 20 kg), the atmospheric density ($\pm 25\%$), the speed of sound ($\pm 10\%$), the drag and lift coefficient ($\pm 20\%$), and in this case also the entry velocity (± 20 m/s) and entry flight-path angle ($\pm 0.1^{\circ}$) all with a uniform distribution. A total of 500 simulations will be performed.

The results of the simulations are presented in Fig. 17 for the same performance indices as before. Despite the larger errors, the results are surprisingly good and sometimes even better than before. The integrated heat load and flight range are the same as before, despite the larger errors. A possible explanation is that now also the nominal guidance is more actively involved in changing the nominal guidance profile, driven by the uncertainties in initial conditions. The heat-flux tracking has become even more efficient compared to Fig. 15, judging the almost absence of the undershoot trajectories and the same maximum overshoot.

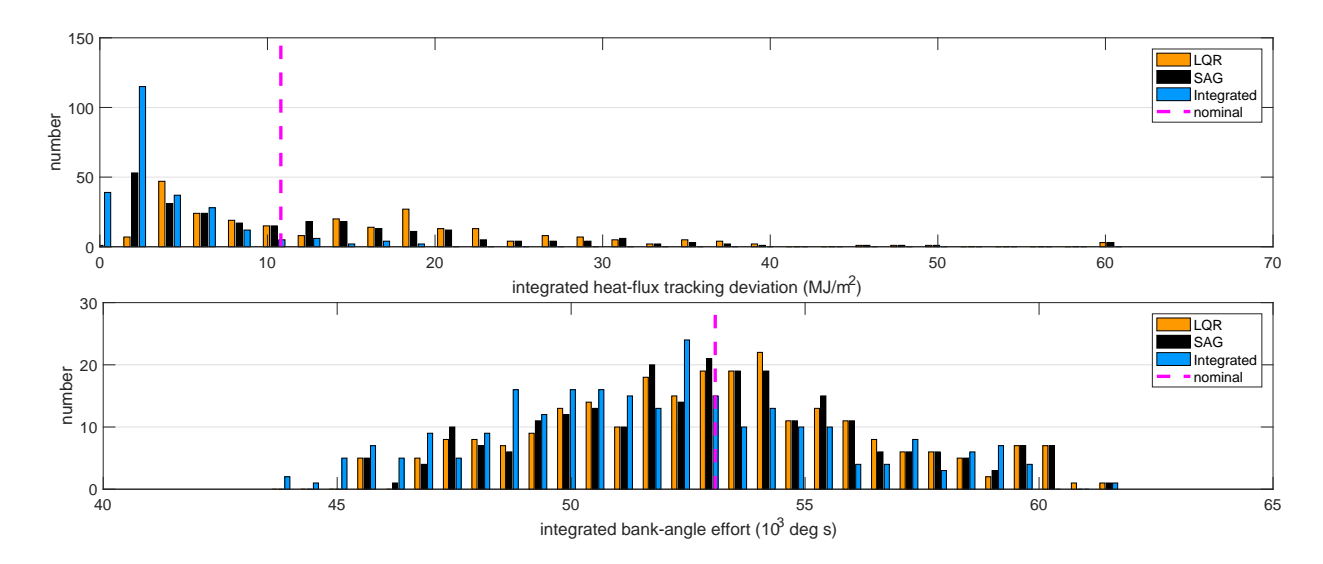


Figure 16. Integrated heat-flux tracking deviation and bank-angle effort for sensitivity analysis (250 runs).

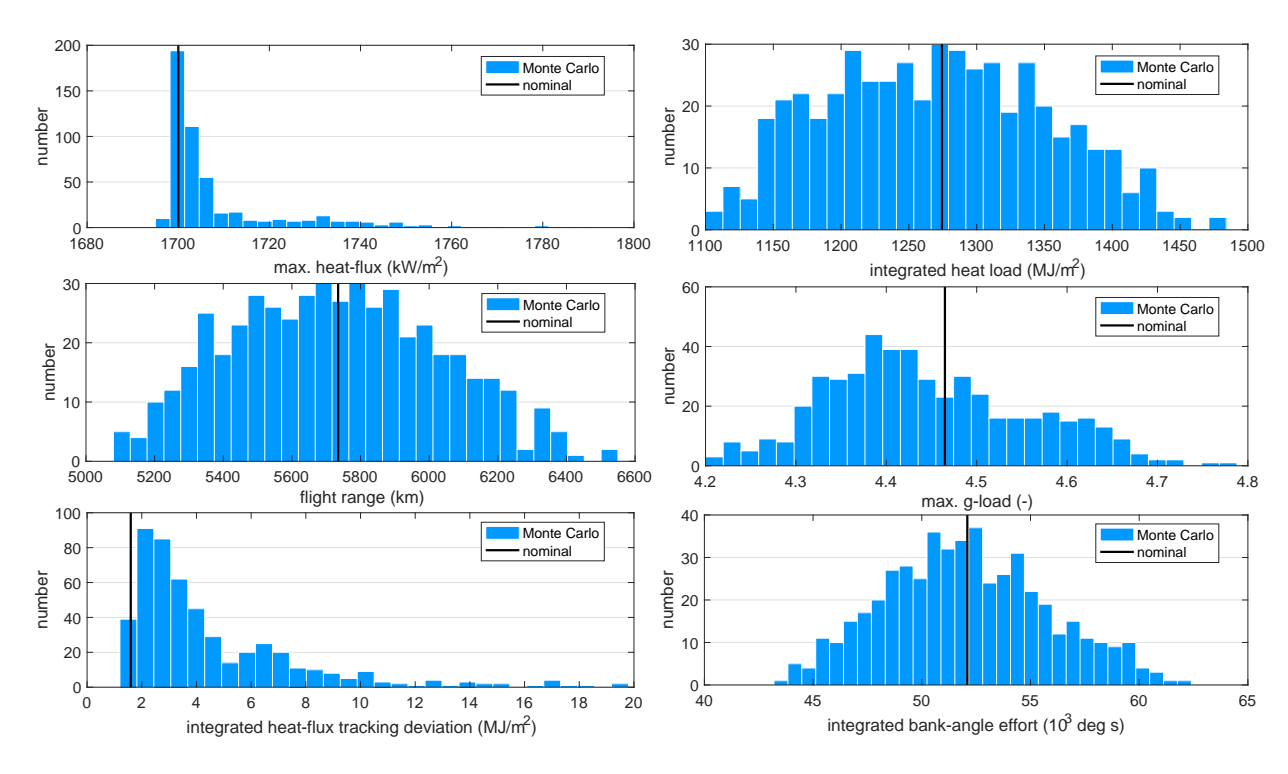


Figure 17. Performance indices for a Monte-Carlo analysis with severe perturbations (500 runs, integrated tracking).

The integrated tracking error has substantially improved, and the reason that it has not further reduced Q is most likely due to the fact that the flight time has somewhat increased and counteracted that. Finally, the integrated bank-angle effort is the same as before. All in all, an excellent result that encourages further development of this guidance configuration.

VI. Conclusions and Recommendations

In this paper the heat-flux tracking for a hypersonic test vehicle called *Hyperion-1*, is studied. Tracking is done by either a (linear) output-feedback controller (LQY), an adaptive tracker based on simple adaptive

control theory (SAG, simple adaptive guidance), or a combination of both (an inner-loop nominal guidance with LQY tracking, and an outer-loop SAG tracking). Changes in the nominal guidance as well as the tracking system have improved the performance with respect to earlier results. These improvements deal with the transition from heat-flux tracking to constraining the maximum g-load using a smooth step function, a PID regulator on the flight-path angle error, a PD regulator on the heat-flux error, and a "smoother" on the heat-flux error towards the end of the tracking phase. Both the heat-flux and g-load constraints are well observed, and the integrated heat-load variation is well within the margins that can be expected during the conceptual-design phase.

The analysis of the guidance system has been done in three steps. In the first step the nominal guidance system has been addressed. Variations in initial conditions, vehicle mass, entry angle-of-attack and angle of attack for maximum cross range, and the set points for maximum heat flux and *g-load*, showed that the guidance is robust. For relatively large variations all guidance profiles resulted in stable trajectories. The occurring peak heat flux was mainly due to the vehicle limitations and not because of a deficiency in the nominal guidance. Including an output tracker in the loop improved the results even more, and reduced the deviations from the nominal profiles.

In the second step, the nominal guidance in combination with all tracking systems was evaluated for uncertainties in the aerodynamic coefficients, vehicle mass, atmospheric density and speed of sound. A Monte Carlo analysis showed that even though there was a 20% variation in both integrated heat load and total flight range, the trajectories were all stable and exhibited only a 5% heat-flux constraint violation. The maximum g-load was observed in all cases. This can be considered a good performance result, because of the slow trajectory dynamics and representative range of perturbations. The LQY and SAG performed almost the same, with a slightly better performance of the SAG. The integrated system performed better than the two apart, and provides a robust guidance system. However, due to physical conflicts the integrated heat load can only be lowered at the expense of a decrease in total flight range, so these objectives need to be balanced once a proper performance optimisation is done.

The third step consisted of another Monte-Carlo analysis with more pronounced perturbations, as well as errors in the initial conditions. This batch was done for the integrated system only. The results were even better than the ones obtained in step 2. An effective combination of an active nominal guidance system in combination with the tracking systems has provided a stable and robust guidance solution for path-constraint tracking.

Future work aims at a more detailed error analysis and extending the number of perturbations in the Monte-Carlo runs. A proper design methodology, starting from actual performance requirements and meeting those with a robust path-constraint tracking system is the final goal of the work. Once the guidance system has been fully developed it would be interesting to test it for other vehicles as well.

References

¹Kaufman, H., Barkana, I. and Sobel, K., *Direct adaptive control algorithms: Theory and applications*, Second edition, Springer-Verlag, New York, 1998.

²Barkana, I., "Classical and Simple Adaptive Control for Non-Minimum Phase Autopilot Design", *Journal of Guidance*, Control, and Dynamics, Vol. 24, No. 4, pp. 631-638, July-August 2004.

³Mooij, E., "Simple Adaptive Bank-Reversal Control of a winged Re-entry Vehicle", AIAA-04-4869, AIAA Guidance, Navigation, and Control Conference, Providence, RI, August 16-19, 2004.

⁴Mooij, E., "Adaptive Heat-Flux Tracking for Re-entry Guidance", AIAA-2014-4142, AIAA/AAS Astrodynamics Specialist Conference, San Diego, CA, August 4-7, 2014.

⁵Mooij, E., "Re-entry Guidance for Path-Constraint Tracking", AIAA-2017-1265, AIAA SciTech 2017, Guidance, Navigation, and Control Conference, Dallas, TX, January 6-10, 2017.

⁶Mooij, E., Maree, A.G.M. and Sudmeijer, K.J., "Aerodynamic controllability of a selected re-entry test vehicle", IAF-95-V.4.04, 46th International Astronautical Congress, Oslo, Norway, October 2-6, 1995.

⁷Vinh, N.X., Optimal trajectories in atmospheric flight, Elsevier scientific publishing company, 1981.

⁸Ebert, D.S., Musgrave, F.K., Peachey, D., Perlin, K., and Worley, S., *Texturing & Modeling: A Procedural Approach*, Third Edition, Ch. 12, "Noise, Hypertexture, Antialiasing, and Gesture", Morgan Kaufmann Publishers, 2003.

⁹Mooij, E., "Passivity Analysis for Non-Linear, Non-Stationary Entry Capsules", *International Journal of Adaptive Control and Signal Processing*, Vol. 28, 2014, pp. 708-731. doi: 10.1002/acs.2386 (published online 2013).